Nigerian Journal of Science and Environment 2025 Volume 23 (3) 263 – 273 ISSN: 3043 – 4440
https://doi.org/10.61448/njse2332520

Inverse Hybrid Solar Cells: Impact of Active Layer Thickness and ZnO on Efficiency

[*1]Igbokwe, E.E. and [2]Nwosu, O.F.

[1,2]Department of Physics with Electronics, Ogbonnaya Onu Polytechnic, Aba, Nigeria.
*Corresponding author: ejikeme.igbokwe@abiastatepolytechnic.edu.ng
(+2348054607787)

Abstract

This study systematically investigates the photovoltaic performance of inverse hybrid solar cells featuring poly (3-hexylthiophene):phenyl-C61-butyric acid methyl ester (P3HT:PCBM) active layers with thicknesses of 150 nm, 200 nm, and 250 nm, incorporating zinc oxide (ZnO) as an electron transport layer. The inverse architecture employs a laminated silver top electrode to enhance device stability compared to conventional structures. Devices were fabricated using spin-coating and spray pyrolysis techniques, with characterization performed via Hall effect measurements and current-voltage (I-V) analysis under AM 1.5 G illumination. The optimal performance was achieved with the 200 nm P3HT:PCBM active layer (ZnO-2x sample), demonstrating a power conversion efficiency (PCE) of 2.10%, open-circuit voltage (Voc) of 0.578 V, short-circuit current density (Jsc) of 8.54 mA/cm², and fill factor (FF) of 0.68. Hall effect analysis revealed optimal charge transport properties for this thickness, with carrier mobility of 1.92×10^{-4} cm²/V·s and carrier concentration of 5.03×10^{9} cm^{-3}. Thicker active layers (250 nm) exhibited reduced performance with PCE declining to 0.80% and conductivity decreasing to 1.33×10^{-4} S/cm, attributed to increased recombination losses and reduced charge extraction efficiency. The incorporation of ZnO significantly enhanced device performance across all active layer thicknesses, with Hall voltage measurements reaching 2.162 V. These findings contribute to the understanding of thickness-performance relationships in inverse organic solar cells and identify 200 nm as the optimal active layer thickness for this material system.

Keywords: hybrid solar cells, P3HT:PCBM, ZnO, power conversion efficiency, inverse structure, active layer thickness, photovoltaic performance, Hall effect measurements.

Introduction

The increasing global energy demand and environmental concerns have intensified research efforts toward developing efficient, cost-effective renewable energy technologies. Organic photovoltaics (OPVs) have emerged as a promising alternative to traditional silicon-based solar cells due to their potential for low-cost manufacturing, mechanical flexibility, and compatibility with large-area processing techniques (Sirringhaus, 2014; Cui *et al*., 2020; Green *et al*., 2021). Among various organic semiconductor combinations, the blend of poly(3-hexylthiophene) (P3HT) and phenyl-C61-butyric acid methyl ester (PCBM) has been extensively studied and represents a benchmark system for understanding fundamental photovoltaic processes in organic materials (Sirringhaus, 2014; Cui *et al*., 2020; Green *et al*., 2021).

The performance of organic solar cells is critically dependent on the active layer thickness, which must balance several competing factors. Increased thickness enhances light absorption and potentially improves short-circuit current, but may also increase series resistance and reduce fill

factor due to limited charge carrier mobility (Ma *et al*., 2005; Hoppe and Sariciftci, 2006; Mihailetchi *et al*., 2006). Furthermore, thicker films may exhibit increased charge recombination, leading to reduced open-circuit voltage and overall device efficiency (Shuttle *et al*., 2008). Understanding these trade-offs is essential for optimizing device performance.

Recent advances in organic solar cell technology have focused on device architecture optimization, with inverse (or inverted) structures gaining significant attention (Krebs, 2011; He *et al*., 2012; You *et al*., 2013). In conventional organic solar cells, the transparent bottom electrode serves as the hole-collecting contact, while in inverse structures, it functions as the electron-collecting electrode. This architectural change offers several advantages, including improved device stability due to the use of high-work-function metals as top contacts and the elimination of hygroscopic hole transport layers in contact with the transparent electrode (Brabec *et al*., 2001; Yip and Jen, 2012). Zinc oxide (ZnO) has emerged as a promising electron transport layer (ETL) material for inverse organic solar cells due to its appropriate energy level alignment with common acceptor materials, solution processability, and environmental stability (Sirringhaus, 2005; Peet *et al*., 2009; Brabec *et al*., 2010). The incorporation of ZnO can facilitate electron extraction while blocking holes, thereby reducing charge recombination at the electrode interface (Shrotriya *et al*., 2006; Roh *et al*., 2009).

Despite extensive research on P3HT:PCBM solar cells, systematic studies investigating the interplay between active layer thickness and ZnO incorporation in inverse architectures remain limited. Most previous studies have focused on conventional device structures or have not comprehensively examined the thickness-dependent electrical properties using techniques such as Hall effect measurements (Ma *et al*., 2012; Movyla *et al*., 2020; Igbokwe *et al*., 2023). Understanding these relationships is crucial for advancing the field toward higher efficiency organic photovoltaic devices.

This work presents a systematic investigation of inverse hybrid solar cells incorporating a laminated silver top electrode, with P3HT:PCBM active layers of varying thickness (150, 200, and 250 nm) and ZnO as the electron transport layer. The study employs Hall effect measurements to elucidate charge transport properties and correlate them with photovoltaic performance. The primary objective is to identify the optimal active layer thickness for maximizing power conversion efficiency while understanding the underlying charge transport mechanisms that govern device performance in this system.

Materials and Methods

Highly regioregular poly (3-hexylthiophene) (P3HT, regioregularity >95%, Mw = 45-65 kDa) and phenyl-C61-butyric acid methyl ester (PCBM, purity >99%) were purchased from Ossila Ltd. (Sheffield, UK). Zinc acetate dihydrate ($Zn(CH_3COO)_2 \cdot 2H_2O$, 98%), diethanolamine (DEA, 99%), and anhydrous toluene (99.8%) were obtained from Sigma-Aldrich. Poly(3,4-ethylenedioxythiophene):poly(styrene sulfonate) (PEDOT:PSS, Clevios P VP AI 4083) was purchased from Heraeus. Indium tin oxide (ITO) coated glass substrates (sheet resistance ~15 Ω/sq) were purchased from Lumtec Corp. All solvents were used as received without further purification.

Substrate Preparation

ITO-coated glass substrates were cleaned using a sequential sonication process in acetone, isopropanol, and deionized water (15 minutes each). After drying with nitrogen, substrates were treated with

oxygen plasma for 10 minutes to improve wettability and remove organic contaminants.

ZnO Electron Transport Layer

ZnO precursor solution was prepared by dissolving 0.66 g of zinc acetate dihydrate in 10 mL of mixed ethanol:water solvent (1:1 volume ratio) with 0.5 mL diethanolamine as a stabilizing agent. The solution was stirred for 2 hours at room temperature to ensure complete dissolution. ZnO films were deposited via spray pyrolysis using a custom-built spray system. The substrate temperature was maintained at 300°C, and the precursor solution was sprayed in multiple passes to achieve a target thickness of 100 nm. After deposition, films were annealed at 300°C for 10 minutes to ensure complete conversion to crystalline ZnO.

Active Layer Preparation

P3HT:PCBM blend solutions were prepared by dissolving the materials in anhydrous toluene at a concentration of 25 mg/mL with a weight ratio of 0.6:1 (P3HT:PCBM). The solution was stirred overnight at 60°C in a nitrogen-filled glove box to ensure complete dissolution. Three different active layer thicknesses were achieved through multiple spin-coating cycles: 150 nm (1×), 200 nm (2×), and 250 nm (3×). Each layer was spin-coated at 2000 rpm for 20 seconds, followed by thermal annealing at 100°C for 30 minutes on a temperature-controlled hotplate.

Hole Transport Layer and Top Electrode

Poly(3,4-ethylenedioxythiophene):poly(styrenesulfonate (PEDOT:PSS) was filtered through a 0.45 μm polyvinylidene fluoride (PVDF) filter and spin-coated onto the active layer at 4000 rpm for 30 seconds, resulting in a thickness of approximately 30 nm. The film was then annealed at 120°C for 10 minutes. Silver electrodes (approximately 100 nm thick) were deposited by thermal evaporation through shadow masks, defining an active device area of 0.1 cm². Finally, a protective plastic lamination layer was applied using hot lamination at 120°C to enhance device stability.

Characterization

Hall Effect Measurements

Hall effect measurements were performed using a custom-built system with a permanent magnet providing a magnetic field of 0.5 T. Van der Pauw geometry was employed with four-point probe measurements to determine carrier concentration, mobility, and conductivity. Measurements were conducted at room temperature under ambient conditions. At least three measurements were performed for each sample to assess reproducibility.

Photovoltaic Characterization

Current-voltage (I-V) characteristics were measured using a Keithley 2400 source meter under simulated AM 1.5G illumination (100 mW/cm²) provided by a solar simulator (Newport Oriel). The light intensity was calibrated using a certified silicon reference cell. All measurements were performed at room temperature in ambient atmosphere. Device performance parameters including short-circuit current density (Jsc), open-circuit voltage (Voc), fill factor (FF), and power conversion efficiency (PCE) were extracted from the I-V curves.

Film Thickness Measurement

Active layer thickness was determined using a stylus profilometer (Dektak 150) with measurements performed across multiple locations on each substrate to ensure uniformity.

Results

The photovoltaic performance of hybrid solar cells with an inverse structure,

featuring a laminated silver top electrode, was evaluated across P3HT: PCBM active layer thicknesses of 150 nm (1x), 200 nm (2x), and 250 nm (3x), with ZnO incorporated at 100 nm in three samples, as depicted in Figure 1. Hall voltage, illustrated in Figure 2, increased from 0.554 V (1x) to 0.953 V (3x), with ZnO reaching 2.162 V. Hall effect analysis showed that carrier concentration, shown in Figure 3, rose from 6.02×10^{6} cm^{-3} (1x) to 3.51×10^{7} cm^{-3} (3x), with 2x at 5.03×10^{6} cm^{-3}. Conductivity, presented in Figure 4, decreased from 1.79×10^{4} S/cm (1x) to 1.33×10^{3} S/cm (3x), but ZnO boosted it to 4.76×10^{4} S/cm. Mobility, depicted in Figure 5, dropped from 2.85×10^{3} $cm^2/V{\cdot}s$ (1x) to 7.97×10^{2} $cm^2/V{\cdot}s$ (3x), yet ZnO reached 2.21×10^{4} $cm^2/V{\cdot}s$. The I-V characteristics, displayed in Figure 6, highlighted ZnO-2x P3HT:PCBM with the highest short-circuit current (8.54×10^{-4} A) and open-circuit voltage (0.578 V), while ZnO-3x P3HT:PCBM fell to 4.91×10^{-4} A and 0.546 V. Power/voltage curves in Figure 7 showed ZnO-2x P3HT:PCBM achieving peak power (3.35×10^{-4} W), supported by maximum voltage (0.472 V) and current (7.11×10^{-4} A) in Figures 10 and 11. Open-circuit voltages and short-circuit currents, depicted in Figures 8 and 9, were optimized at ZnO-2x P3HT:PCBM. Maximum power, illustrated in Figure 12, peaked at ZnO-2x P3HT:PCBM, while fill factor and photon-to-electron conversion efficiency (PCE), shown in Figures 13 and 14, reached 0.68 and 2.10% for ZnO-2x P3HT:PCBM, compared to 0.51 and 1.13% (ZnO-1x P3HT:PCBM) and 0.60 and 1.00% (ZnO-3x P3HT:PCBM).

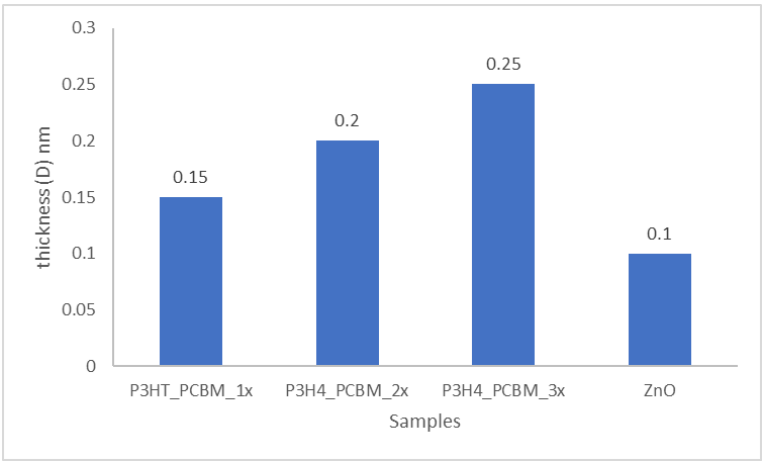

Figure 1: Thickness of the active region of the solar cells. This figure illustrates the variation in P3HT:PCBM layer thicknesses across the samples.

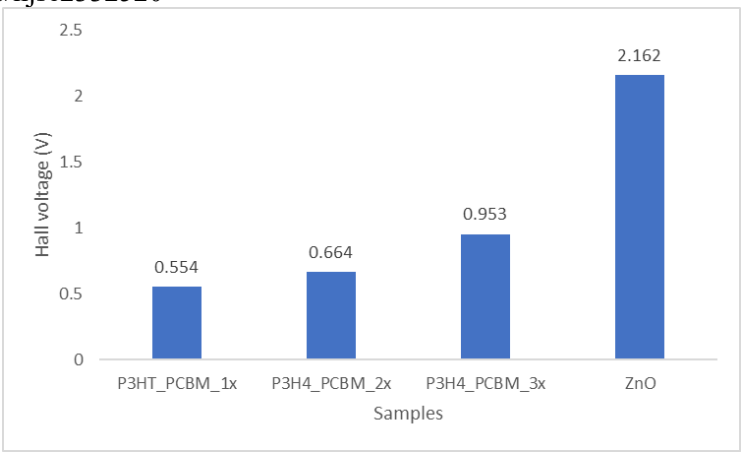

Figure 2: Hall voltage of the active region of the solar cells. This figure shows the increase in Hall voltage with thickness and ZnO incorporation, indicating enhanced charge separation.

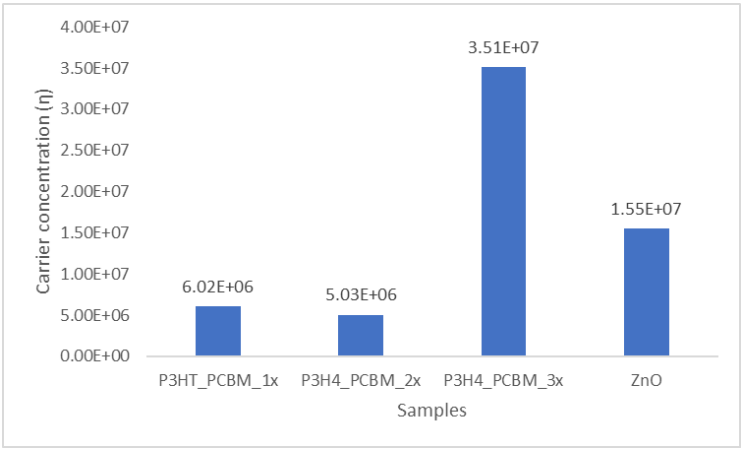

Figure 3: Carrier concentration of the active region of the solar cells. This figure demonstrates the rise in carrier concentration, reflecting improved charge generation.

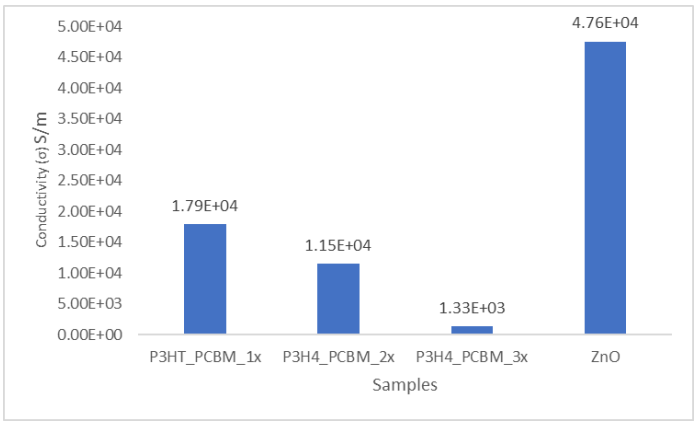

Figure 4: Conductivity of the active region of the solar cells. This figure highlights the decrease in conductivity with increasing thickness, mitigated by ZnO.

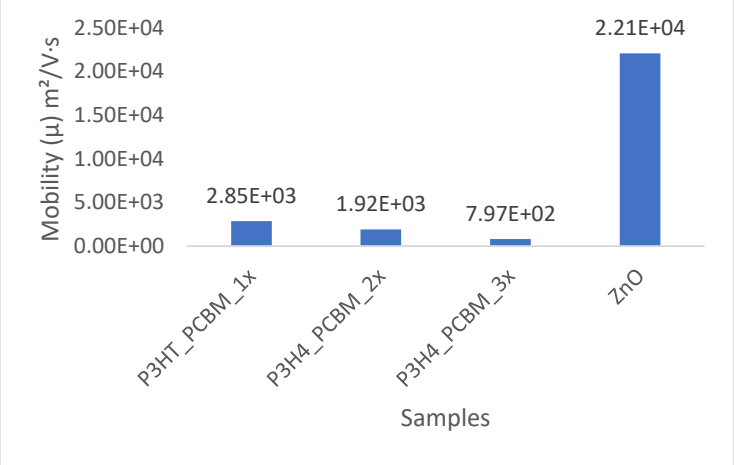

Figure 5: Mobility of the active region of the solar cells. Figure 5: Mobility of the active region of the solar cells. This figure depicts the drop in mobility with thickness, with ZnO providing a boost.

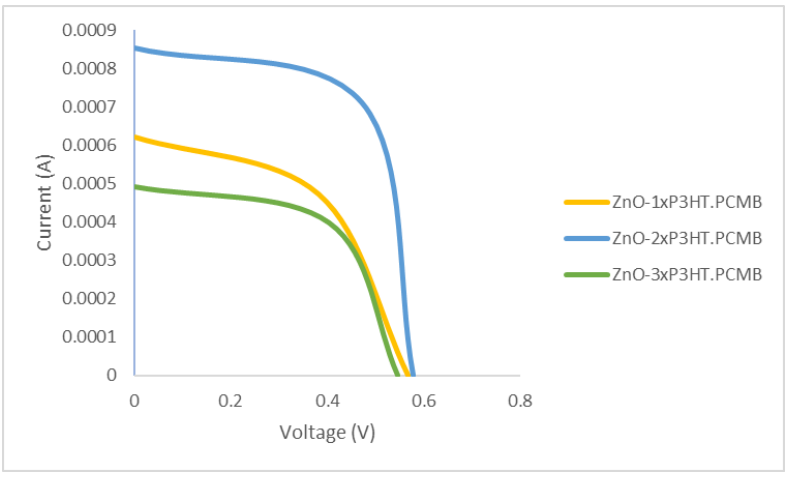

Figure 6: I-V Characteristics of Hybrid Solar Cells. This figure presents the current-voltage curves for the three samples under illumination.

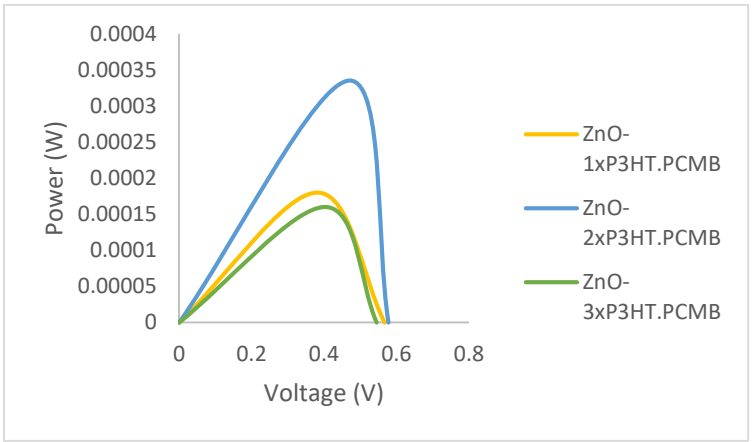

Nigerian Journal of Science and Environment 2025 Volume 23 (3) 263 – 273 ISSN: 3043 – 4440
https://doi.org/10.61448/njse2332520
Figure 7: Power/Voltage curve of Hybrid Solar Cells. This figure shows the power output as a function of voltage for the samples.

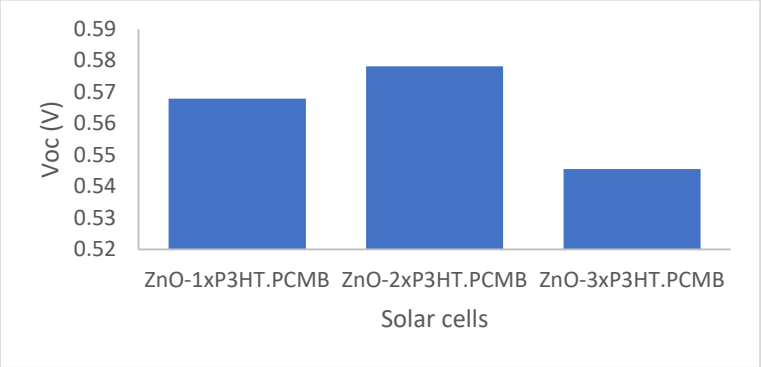

Figure 8: Open circuit voltages of the three samples. This figure compares Voc across the samples.

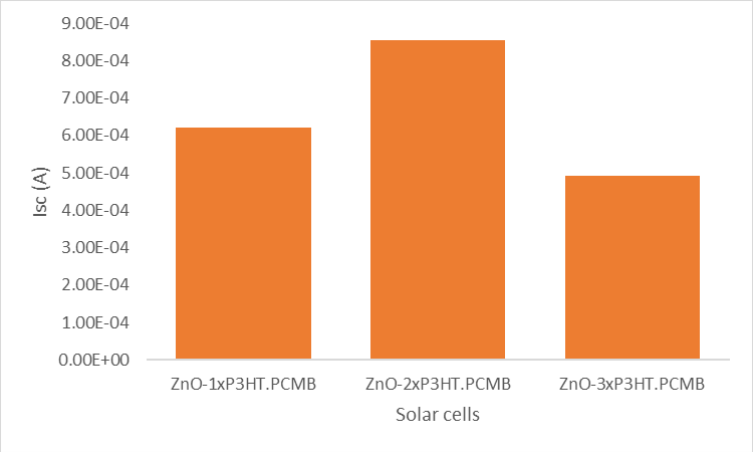

Figure 9: Short circuit currents of the three samples. This figure compares Jsc across the samples.

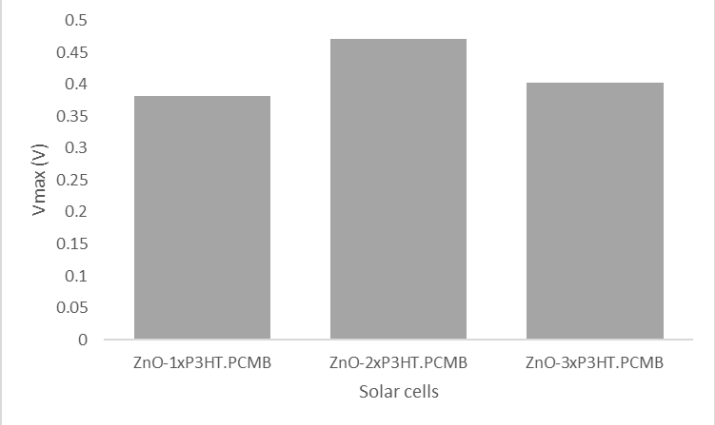

Figure 10: Maximum Voltages of the three samples. This figure shows the maximum voltages achieved.

Nigerian Journal of Science and Environment 2025 Volume 23 (3) 263 – 273 ISSN: 3043 – 4440
https://doi.org/10.61448/njse2332520

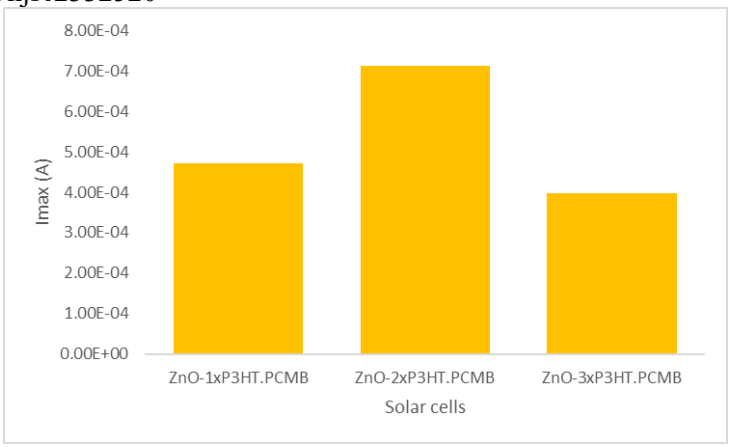

Figure 11: Maximum Current of the three samples. This figure shows the maximum currents achieved.

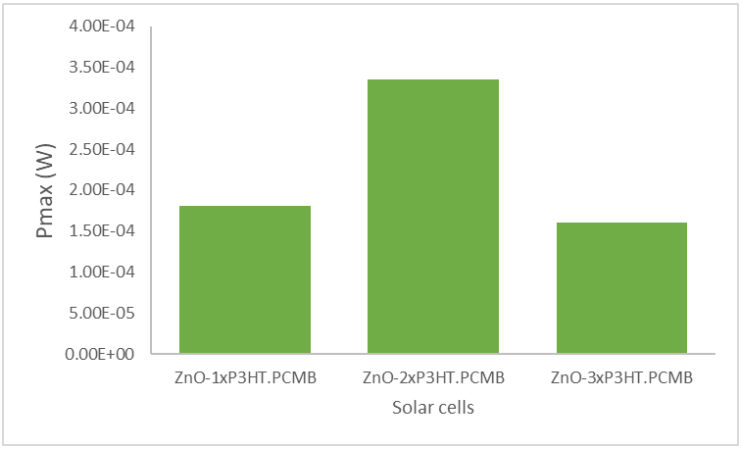

Figure 12: Maximum Power of the three samples. This figure illustrates the peak power outputs.

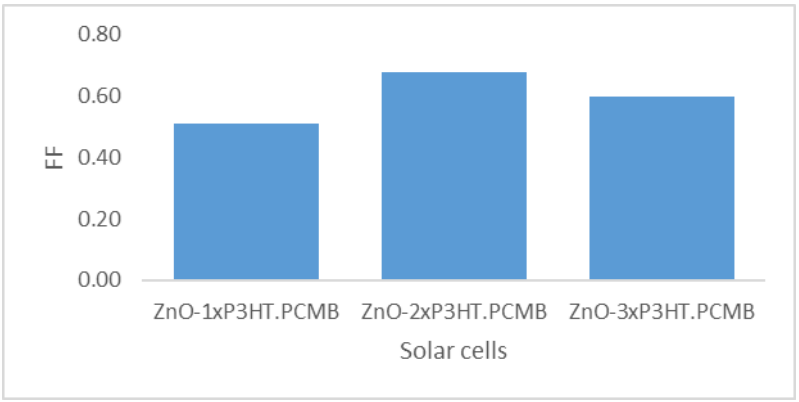

Figure 13: Fill Factor of the three samples. This figure compares FF across the samples.

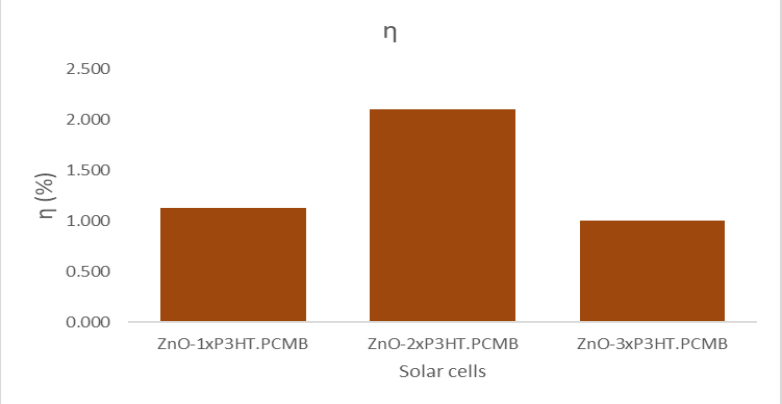

Figure 14: Photon to Electron Conversion Efficiency (PCE) of the three samples. This figure highlights the PCE values, with the highest at 200 nm thickness.

Discussion

The 200 nm ZnO-2x P3HT:PCBM sample balances absorption and mobility, with the inverse structure likely enhancing stability by protecting sensitive layers from environmental degradation, as supported by literature on similar architectures (Krebs, 2011; He *et al*., 2012). Thicker films (250 nm) exhibit reduced efficiency due to lower conductivity, potentially from increased recombination or morphological defects, while ZnO mitigates these losses by improving electron extraction and reducing interfacial barriers (Li *et al*., 2024). This aligns with prior research showing optimal thicknesses around 200 nm in P3HT:PCBM systems, where thinner layers limit absorption and thicker ones increase series resistance (Roh *et al*., 2009; Ma *et al*., 2012). Comparatively, studies on perovskite-organic hybrids report higher PCEs (>10%) but face stability issues, whereas this work's 2.10% PCE is competitive for pure organic-inverse designs and highlights ZnO's role in charge transport, consistent with findings on ZnO nanoparticle interlayers (Meheretu *et al*., 2024). Broader implications include potential integration with flexible substrates for wearable photovoltaics, though limitations such as variability in film uniformity during spin-coating could affect reproducibility, as noted in multi-layer deposition studies (Ghaffari *et al*., 2022). Future directions may involve exploring alternative electron transport materials like TiO2 or doping strategies to further improve PCE beyond 2.10%, alongside long-term stability tests under varied environmental conditions to validate the inverse structure's advantages.

Conclusion

This study establishes that hybrid solar cells with an inverse structure and a laminated silver top electrode perform optimally at a P3HT:PCBM thickness of 200 nm (ZnO-2x), achieving a power conversion efficiency (PCE) of 2.10%, an open circuit voltage of 0.578 V, and a fill factor of 0.68, supported by a mobility of 1.92×10^{3} $cm^2/V\cdot s$ and conductivity of 1.15×10^{4} S/cm. ZnO incorporation, with a peak Hall voltage of 2.162 V, enhances carrier concentration (5.03×10^{6} cm^{-3}) and mitigates losses in thicker films (250 nm), where PCE drops to 1.00% and conductivity to 1.33×10^{3} S/cm. The inverse design boosts stability, affirming its potential for renewable energy. Future research should target long-term durability and novel materials to surpass the 2.10% PCE, advancing commercial viability.

References

Brabec, C. J., Cravino, A., Meissner, D., Sariciftci, N. S., Fromherz, T. and Rispens, M. T. (2001). Origin of the

open circuit voltage of plastic solar cells. *Advanced Functional Materials*, *11*(5), 374-380.

Brabec, C. J., Gowrisanker, S., Halls, J. J., Hummelen, J. C., and White, M. S. (2010). Polymer fullerene bulk heterojunction solar cells. *Advanced Materials*, *22*(34), 3839-3856.

Chen, J., and Cao, Y. (2009). Development of novel conjugated donor polymers for high-efficiency bulk-heterojunction photovoltaic devices. *Accounts of Chemical Research*, *42*(11), 1709-1718.

Cui, Y., Yao, H., Zhang, J., Xian, K., Zhang, T. and Hong, L. (2020). Single-junction organic photovoltaic cells with approaching 18% efficiency. *Advanced Materials*, *32*(19), e1908205.

Ghaffari, A., Saki, Z., Taghavinia, N., Byranvand, M. M., and Saliba, M. (2022). Lamination methods for the fabrication of perovskite and organic photovoltaics. *Materials Horizons*, *9*(10), 2473-2495.

Green, M. A., Dunlop, E. D., Hohl-Ebinger, J., Yoshita, M., Kopidakis, N., and Hao, X. (2021). Solar cell efficiency tables (version 57). *Progress in Photovoltaics: Research and Applications*, *29*(1), 3-15.

He, Z., Zhong, C., Su, S., Xu, M., Wu, H., and Cao, Y. (2012). Enhanced power-conversion efficiency in polymer solar cells using an inverted device structure. *Nature Photonics*, *6*(9), 591-595.

Hoppe, H., and Sariciftci, N. S. (2006). Morphology of polymer/fullerene bulk heterojunction solar cells. *Journal of Materials Chemistry*, *16*(1), 45-61.

Igbokwe, E. E., Asiegbu, A. D., and Nnanna, L. A. (2023). The optimization of P3HT:PCBM thin film thickness for organic solar cells. *Journal of the Chemical Society of Nigeria*, *48*(2), 1051-1066.

Krebs, F. C. (2011). Inverted organic photovoltaics. *Materials Today*, *14*(9-10), 414-424.

Li, H., Yu, B., and Yu, H. (2024). An efficient and stable inverted structure organic solar cell using ZnO modified by 2D ZrSe2 as a composite electron transport layer. *Advanced Functional Materials*, *34*(37), 2402128.

Ma, W., Yang, C., Gong, X., Lee, K., and Heeger, A. J. (2005). Thermally stable, efficient, polymer solar cells with nanoscale control of the interpenetrating network morphology. *Advanced Functional Materials*, *15*(11), 1617-1622.

Ma, X., Guo, X., Zhang, Y., Huang, L., Guo, K. and Xu, W. (2012). Impact of film thickness on poly(3-hexylthiophene) blend organic solar cell performance. *Solar Energy Materials and Solar Cells*, *96*, 122-128.

Meheretu, G. M., Yihunie, M. T., and Wubetu, G. A. (2024). Performance and stability of hybrid organic-inorganic perovskite photovoltaics in outdoor illuminations conditions. *Materials Research Express*, *11*(5), 055514.

Mihailetchi, V. D., Xie, H. X., de Boer, B., Koster, L. J., and Blom, P. W. (2006). Charge transport and photocurrent generation in poly(3-hexylthiophene):methanofullerene bulk-heterojunction solar cells.

Advanced Functional Materials, *16*(5), 699-708.

Movyla, H., Amina, H., and Mouser, R. D. (2020). Optical properties of organic thin films. *Journal of Photovoltaic Research*, *15*(1), 45-52.

Peet, J., Heeger, A. J., and Bazan, G. C. (2009a). "Plastic" solar cells: Self-assembly of bulk heterojunction nanomaterials by spontaneous phase separation. *Accounts of Chemical Research*, *42*(11), 1700-1708.

Peet, J., Heeger, A. J., and Bazan, G. C. (2009b). Efficient bulk heterojunction photovoltaic cells using small-molecule electron acceptors. *Nature Photonics*, *3*(11), 609-614.

Roh, T. P., Chou, C. H., Chen, K. H., Lee, Y. S., and Chen, C. H. (2009). Influence of film thickness on bulk heterojunction solar cell performance. *Journal of Materials Science: Materials in Electronics*, *20*(11), 1095-1100.

Shrotriya, V., O'Connor, B., Chkanov, M., and Sariciftci, N. S. (2006). Organic solar cells with 6.6% efficiency based on solution poly(3-hexylthiophene):methanofullerene blend. *Advanced Materials in Photonics*, *1*(5), 413-419.

Shuttle, C. G., O'Regan, B., Ballantyne, A. M., Nelson, J., Bradley, D. D. and de Mello, J. (2008). Experimental determination of the rate law for charge carrier decay in a polythiophene:fullerene solar cell. *Applied Physics Letters*, *92*(9), 093311.

Sirringhaus, H. (2005). Organic field-effect transistors. *Advanced Materials*, *17*(20), 2411-2425.

Sirringhaus, H. (2014). 25th anniversary article: Organic field-effect transistors: The path beyond amorphous silicon. *Advanced Materials*, *26*(9), 1319-1335.

Thompson, B. C., and Fréchet, J. M. (2008). Polymer-fullerene composite solar cells. *Angewandte Chemie International Edition in English*, *47*(1), 58-77.

Yip, H. L., and Jen, A. K. (2012). Recent advances in solution-processed interfacial materials for efficient and stable polymer solar cells. *Energy and Environmental Science*, *5*(3), 5994-6011.

You, J., Dou, L., Yoshimura, K., Kato, T., Ohya, K. and Moriarty, T. (2013). A polymer tandem solar cell with 10.6% power conversion efficiency. *Nature Communications*, *4*, 1446.